truncation of the APC protein (table S1). The complete absence of equivalent mutations in control mice indicates that the suppression of intestinal tumors by *Mbd4* is due at least in part to suppression of CpG → TpG transitions at the endogenous *Apc* gene.

Our findings clearly implicate MBD4 in the repair of m^5C deamination at methylated CpG residues, but is it solely responsible for this repair? If we assume that the in vitro deamination rate of m^5C (5.8×10^{-13}/second) (*2*) applies in vivo, we predict a C → T transition frequency of 1.25×10^{-4} at CpG sites in the *cII* locus in the absence of repair. The observed mutation frequency in wild-type mice is 4% of this calculated value, suggesting that repair of m^5C deamination is about 96% efficient. In *Mbd4*$^{-/-}$ mice, the CpG to TpG mutation frequency is 1.5×10^{-5}, suggesting that repair efficiency has fallen to 88% but remains moderately effective. This approximate calculation indicates that repair of deaminated m^5C is shared with factors other than MBD4, for example, TDG or equivalent activities. In theory, two independent repair activities that were each ~80% efficient could give a combined efficiency of ~96%.

Why is m^5C a mutational hotspot in spite of the presence of at least one repair mechanism? One plausible explanation is that the existence of close to 10^9 T residues in the mouse genome, each one losing its base pairing with A many times per second (*19*), renders enzymes that remove unpaired T potentially mutagenic. With respect to C deamination, this problem is thought to have been solved by replacing U with T in the ancestral RNA-derived genome, so that the deamination product of C became easily distinguishable from a normal DNA base (*20*). All known U:G mismatch glycosylases are inert against T:G mismatches, despite the structural similarity between T and U, perhaps because of the danger of T removal. By methylating C, however, the problem is recreated, as deamination once more generates a normal DNA base whose excision may be problematic. Inefficient correction of the resulting T:G mismatches may represent a compromise between the benefits of repair and the damage that could arise by removal of legitimate T residues.

In conclusion, we have shown that murine MBD4 suppresses CpG → TpG mutations in both a bacteriophage-based transgene and at the endogenous *Apc* gene locus. These findings suggest that human MBD4 plays a similarly important role in reducing inherited disease and cancer.

References and Notes

1. M. Krawczak, E. V. Ball, D. N. Cooper, *Am. J. Hum. Genet.* **63**, 474 (1998).
2. J.-C. Shen, W. M. I. Rideout, P. A. Jones, *Nucleic Acids Res.* **22**, 972 (1994).
3. K. Wiebauer, J. Jiricny, *Nature* **339**, 234 (1989).
4. P. Neddermann, J. Jiricny, *J. Biol. Chem.* **268**, 21218 (1993).
5. B. Hendrich, U. Hardeland, H.-H. Ng, J. Jiricny, A. Bird, *Nature* **401**, 301 (1999).
6. F. Petronzelli *et al.*, *J. Biol. Chem.* **275**, 32422 (2000).
7. B. Hendrich, A. Bird, *Mol. Cell. Biol.* **18**, 6538 (1998).
8. F. Petronzelli *et al.*, *J. Cell. Physiol.* **185**, 473 (2000).
9. Materials and methods are available as supporting material on *Science* Online.
10. J. Guy, unpublished observations.
11. S. W. Kohler *et al.*, *Proc. Natl. Acad. Sci. U. S. A.* **88**, 7958 (1991).
12. J. L. Jakubczak *et al.*, *Proc. Natl. Acad. Sci. U. S. A.* **93**, 9073 (1996).
13. P. R. Harbach, D. M. Zimmer, A. L. Filipunas, W. B. Mattes, C. S. Aaron, *Environ. Mol. Mutagen.* **33**, 132 (1999).
14. A. Riccio *et al.*, *Nature Genet.* **23**, 266 (1999).
15. S. Bader, M. Walker, D. Harrison, *Br. J. Cancer* **83**, 1646 (2000).
16. C. Lengauer, K. W. Kinzler, B. Vogelstein, *Nature* **386**, 623 (1997).
17. L. K. Su *et al.*, *Science* **256**, 668 (1992).
18. C. Luongo, A. R. Moser, S. Gledhill, W. F. Dove, *Cancer Res.* **54**, 5947 (1994).
19. J. L. Leroy, M. Kochoyan, T. Huynh-Dinh, M. Gueron, *J. Mol. Biol.* **200**, 223 (1988).
20. A. Poole, D. Penny, B. M. Sjoberg, *Nature Rev. Mol. Cell. Biol.* **2**, 147 (2001).
21. C. B. Millar, unpublished observation.

22. We thank C. Abbott for advice, D. Macleod for comments on the manuscript, H. Barr for DNA sequencing, N. Hill and the staff of the Anne Walker Building for animal husbandry. Supported by the Cancer Research Campaign and by a Programme Grant from the Wellcome Trust. C.B.M. holds a Wellcome Trust 4-year Ph.D. Studentship. A.R.C. is a Royal Society University Research Fellow.

Supporting Online Material

www.sciencemag.org/cgi/content/full/297/5580/403/DC1
Materials and Methods
Fig. S1
Table S1

29 April 2002; accepted 18 June 2002

A Role for Peroxisomes in Photomorphogenesis and Development of *Arabidopsis*

Jianping Hu,[1,2] Maria Aguirre,[1,2] Charles Peto,[3] José Alonso,[1] Joseph Ecker,[1] Joanne Chory[1,2]*

The nuclear protein DET1 is a central repressor of photomorphogenesis in plants. We have identified the molecular lesion in *ted3*, a mutation that dominantly suppresses the phenotypes of *det1-1*. *TED3* encodes a peroxisomal protein (AtPex2p) essential for *Arabidopsis* growth. Developmental defects and the abnormal expression of many genes in *det1* are rescued by *ted3*. *ted3* also partially suppresses another pleiotropic de-etiolated mutant *cop1*. Thus, peroxisomes, whose functions are still largely unexplored, play a key role in a photomorphogenetic pathway negatively regulated by the DET1 and COP proteins.

Plants use sophisticated signal transduction systems to sense and respond to environmental variation. The light signaling network, for example, consists of a complex web of interactions between multiple photoreceptors, early signaling factors, and central integrators to control the expression of hundreds of responsive genes (*1*). The *Arabidopsis* DET1, COP, and FUS proteins are proposed to be global repressors of photomorphogenesis, because their loss-of-function mutants develop as light-grown plants in the absence of light (*2*). Dark-grown *det1* mutants have short hypocotyls, opened cotyledons, and developed chloroplasts and ectopically express many light-regulated genes (*3*). They also exhibit stress symptoms, such as anthocyanin accumulation and aberrant expression of stress-related genes. Light-grown *det1* plants exhibit general growth defects, such as small, pale-green leaves and seedling lethality in strong alleles (*3*). *DET1* encodes a 62-kD nuclear protein that regulates gene expression (*4*), yet its precise mechanism of action is still unknown.

To better understand how DET1 exerts its functions on photomorphogenesis and development, we identified several extragenic suppressors of *det1-1*, an intermediate-strength allele that is impaired in the splicing of intron 1 but still produces ~2% of wild-type mRNA, and named them *ted* mutants. *ted3* is a dominant suppressor of *det1* phenotypes that does not correct the splicing defect of *det1-1* (*5*).

We fine-mapped the *TED3* gene to a ~130-kb region at the bottom of chromosome 1 (Fig. 1A). Sequencing of selected open reading frames (ORFs) in this interval in *ted3* revealed a mutation in an ORF with 333 amino acids (GenBank accession number AAG52254). Sequence comparison between the genomic fragment and the corresponding expressed sequence tag (EST) clone (N96573) suggested that this gene has eight exons (Fig. 1A) and encodes a 38-kD protein.

[1]Plant Biology Laboratory, [2]Howard Hughes Medical Institute, [3]Laboratory of Neuronal Structure and Function, The Salk Institute for Biological Studies, La Jolla, CA 92037, USA.

*To whom correspondence should be addressed. E-mail: chory@salk.edu

The deduced TED3 protein has a C_3HC_4-type RING finger motif and two putative membrane-spanning domains (Fig. 1, A and C). A transition from G to A in *ted3* caused a missense mutation of a valine to methionine substitution at residue 275, one amino acid upstream of the first cysteine of the putative RING finger domain (Fig. 1, A and C). To confirm that the nucleotide change in *ted3* is responsible for the suppression of *det1-1*, we transformed *det1-1* with a transfer DNA (T-DNA) containing the mutant *ted3* gene with its own flanking sequence (*6*). As shown in Fig. 1B, plants carrying the mutant *ted3* transgene [*det1-1 (ted3)*] were able to recapitulate the suppression phenotypes.

Database searches identified *TED3* as a single-copy gene in *Arabidopsis* that is homologous (~20 to 24% identity) to the yeast and mammalian *PEX2* genes involved in peroxisome assembly and matrix protein import (*7*). An alignment of TED3 with its homologs from human and *Pichia pastoris* showed conserved residues along the length of these proteins (Fig. 1C). Phylogenetic analysis demonstrated that TED3 is more closely related to PEX2 proteins than it is to AtPex10p, the *Arabidopsis* protein most similar (13% identity) to TED3 (Fig. 1D). AtPex10p also contains a RING finger domain and belongs to the PEX10 family of peroxisomal membrane proteins (*7*). AtPex10p and PEX2 proteins are ~10 to 13% identical, suggesting that *PEX2* and *PEX10* are two distantly related gene families.

Present in almost all eukaryotes, peroxisomes are single membrane–bound organelles that perform a wide array of metabolic reactions such as β-oxidation of long-chain fatty acids (*7*). Functions of plant peroxisomes include lipid mobilization via β-oxidation and the glyoxylate cycle for the germination of oilseed (such as *Arabidopsis*) seedlings, photorespiration, and nitrogen metabolism in root nodules (*8*). To determine the localization of TED3/AtPex2p, *Arabidopsis* seedlings containing a TED3::GFP (green fluorescent protein) fusion protein driven by the 35S cauliflower mosaic virus promoter (*9*) were analyzed by fluorescence microscopy. TED3::GFP showed a punctate pattern of green fluorescence, which colocalized with the peroxisomal enzyme catalase (Fig. 2A), indicating that, like its yeast and mammalian counterparts, TED3/AtPex2p is peroxisomal.

Yeast *PEX2* knockouts, in which the *PEX2* gene is disabled, do not grow on alternative carbon sources, such as oleic acid and methanol, whereas analogous knockouts in mammals exhibit severe neurological dysfunctions and infant death (*7*). To study the role of TED3/AtPex2p in plant growth and development, we isolated two independent lines containing a T-DNA insertion in the seventh intron or the eighth exon (the RING finger region) of *TED3* (Fig. 1A). In each case, of the ~200 T2s and T3 progeny from the heterozygous T2s, 2/3 were heterozygous for the insertion and 1/3 had no insertion, whereas no homozygotes were found, sug-

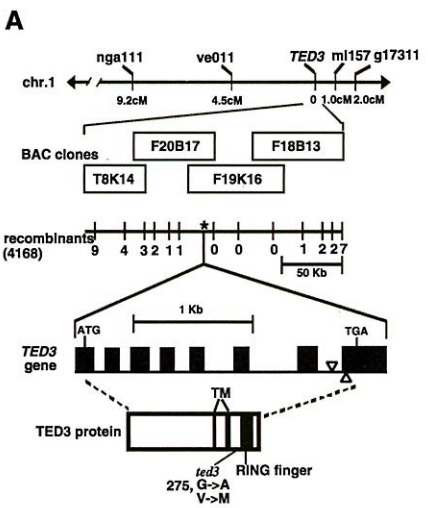

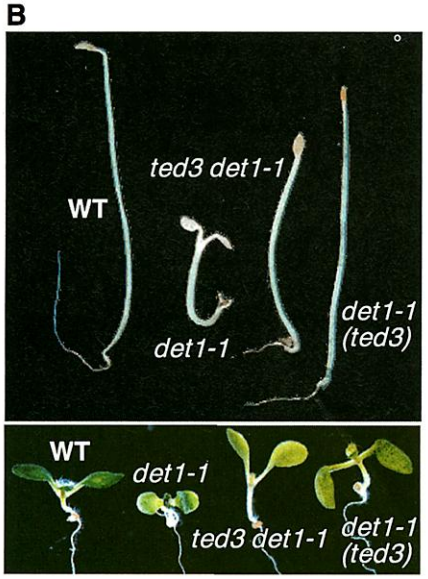

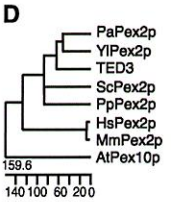

Fig. 1. Cloning and sequence analysis of *TED3*. (**A**) Fine mapping of the *TED3* gene. *TED3* was mapped by analyzing 4168 chromosomes from F_2 plants of *ted3 det1-1* (Col-0) X *Ler* with molecular markers (*22*). In the *TED3* gene, solid lines represent introns, black boxes represent exons, and triangles indicate positions of the T-DNA insertions described in the text. In the TED3 protein, the two putative transmembrane (TM) domains and the RING finger motif are shown as black boxes. The mutation in *ted3* and its position relative to the start codon are indicated. (**B**) Suppression of *det1-1* by the *ted3* transgene. (Top) 6-day-old dark-grown seedlings. (Bottom) 8-day-old light-grown seedlings. (**C**) Alignment of TED3 with HsPex2p (P28328) and PpPex2p (X96945). Black boxes are identical residues; dotted lines indicate gaps. The two putative transmembrane domains in TED3 are underlined. Asterisks denote the conserved cysteine and histidine residues in the RING finger. The arrow indicates the position of the *ted3* mutation. (**D**) Phylogenetic analysis of the relationship between TED3 and other PEX2 proteins. GenBank accession numbers are as follows: PaPex2p, *Podospora anserina*, X87329; YlPex2p, *Yarrowia lipolytica*, U43081; ScPex2p, *Saccharomyces cerevisiae*, M86538; MmPex2p, *Mus musculus*, L27842; AtPex10p, AF119572. Sequence alignment and tree construction were performed with the use of the MegAlign program. The bottom scale indicates relative distance between sequences.

gesting embryonic lethality for the null mutants. This conclusion was reinforced when we observed smaller siliques with fewer seeds in the heterozygotes compared with their siblings without the insertion (Fig. 2B). Also, transgenic plants with the *TED3* antisense construct (*10*) and much reduced *TED3* transcript were dwarf-sized, pale, and sterile (Fig. 2C). *TED3* messenger RNA (mRNA) was detected in all tissues and in light- and dark-grown seedlings (Fig. 2D), indicating that *TED3* is ubiquitously expressed throughout development. Transgenic lines carrying T-DNAs with a fusion of the TED3 promoter and the β-glucuronidase (GUS) reporter gene (*11*) revealed high-level expression of TED3::GUS in cotyledons, pollen, ovules, and seeds (Fig. 2, E to G), suggesting that TED3/AtPex2p is essential for *Arabidopsis* reproduction and development.

Given that ted3::GFP was still peroxisome localized (*12*), we asked whether peroxisomal activities were impaired in *det1* and, if so, whether *ted3* could correct these deficiencies. Because *Arabidopsis* seeds catabolize fatty acids into sugar in glyoxysomes (specialized peroxisomes), the ability to germinate and develop on sugar-free medium primarily reflects peroxisomal activity (*13*). Dark-grown wild-type seedlings on sugar-free medium had longer hypocotyls than on sugar-containing plates due to the inhibition of sucrose on hypocotyl elongation (Fig. 3A), whereas *det1-1* mutants were developmentally arrested without supplemental sugar. Almost all of these *det1-1* seedlings failed to green or grow true leaves even after being transferred to light for 5 days (Fig. 3B). These glyoxysomal deficiencies in *det1-1*, however, could be rescued by *ted3* (Fig. 3, A and B). We also performed a root elongation assay, in which the growth of *det1-1* and *ted3* on IBA (indole-3-butyric acid) was tested. Given that IBA can be converted to IAA (indole-3-acetic acid) in a process similar to β-oxidation in glyoxysomes, β-oxidation mutants would also be defective in the conversion of IBA to IAA and would show resistance to the inhibition of root elongation by IBA (14). *det1-1* did show some degree of resistance to IBA, whereas *ted3 det1-1* and wild-type plants responded to IBA in a similar way (Fig. 3C). Electron micrographs (*15*) showed some morphological differences in *det1-1* peroxisomes. Peroxisomes in light-grown *det1-1* plants usually had a less dense matrix compared with wild-type and *ted3* plants (Fig. 3, D to G), indicating that *det1* might be deficient in peroxisomal matrix proteins. Taken together, we conclude that *det1* seedlings have defective peroxisomes, a trait that can be rescued by the *ted3* gain-of-function mutation. We also crossed *det1* to a loss-of-function peroxisomal mutant *pxa1*, which is defective in transporting fatty acids but has a

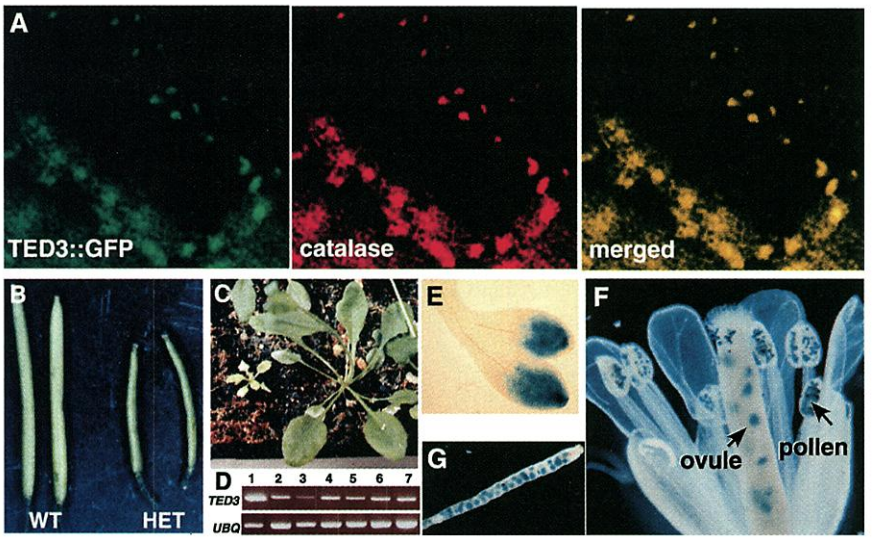

Fig. 2. TED3/AtPex2p is an essential peroxisomal protein. **(A)** Subcellular localization of TED3::GFP. Hypocotyl cells from dark-grown TED3::GFP seedlings were probed with cottonseed catalase antiserum and subsequently with Texas Red–conjugated secondary antibody (*23*). **(B)** Siliques from wild-type and plants heterozygous (HET) for the T-DNA insertion in the *TED3* gene. **(C)** Comparison of 21-day-old plants. (Left) *TED3* antisense line; (right) wild-type. **(D)** Reverse transcriptase–polymerase chain reaction (RT-PCR) analysis of *TED3* (top) and *Ubiquitin10* (bottom) RNA from leaf, flower, silique, stem, root, 5-day light-, and dark-grown seedlings, lanes 1 to 7, respectively. **(E** to **G)** TED3::GUS expression in cotyledons, flower and seeds, respectively.

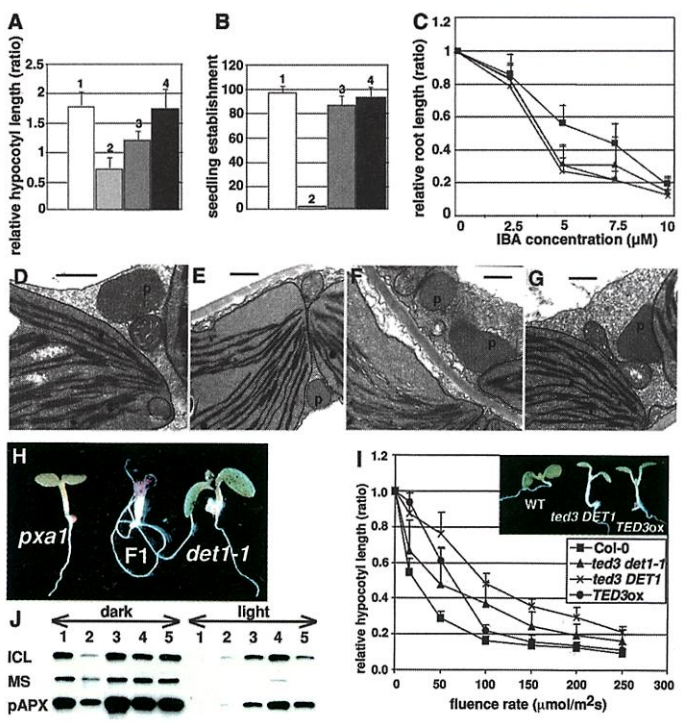

Fig. 3. Peroxisomal defects in *det1-1* are rescued by *ted3*. **(A)** Hypocotyl measurements of 6-day dark-grown seedlings on sugar-free medium. The *y* axis represents mean ratios of hypocotyl length between seedlings grown in the presence of 1.5% sucrose and without it. **(B)** Frequency of seedling establishment (percentage of seedlings that develop true leaves) on sugar-free plates. In (A) and (B), 1 to 4 represent wild-type Col-0, *det1-1*, *ted3 det1-1*, and *ted3 DET1* plants, respectively. **(C)** IBA dose-response curves of 7-day light-grown seedlings. The mean ratios of hypocotyl lengths between seedlings grown with and without IBA were plotted against increasing IBA concentrations. Diamond, Col-0; square, *det1-1*; triangle, *ted3 det1-1*; cross, *ted3 DET1*. **(D** to **G)** Electron micrographs of cotyledon cells from 5-day light-grown seedlings of wild-type, *det1-1*, *ted3 det1-1*, and *ted3 DET1* plants. P, peroxisome. Bars, 0.5 μm. **(H)** Phenotypic comparison of *pxa1*, *det1-1*, and their F_1 progeny grown under ~300 μmol/m²s of white light. **(I)** Fluence rate response curves in white light. Mean ratios of hypocotyl lengths between 7-day-old seedlings grown in white light or complete darkness were plotted against increasing light fluence rates. Inset, 7-day light-grown seedlings. Error bars in (A) to (C) and (I) indicate standard deviations. **(J)** Western blot analysis of glyoxysomal proteins detected by *Arabidopsis* antibody to ICL and antibody to MS and cucumber antibody to pAPX, respectively. Wild-type, *det1-1*, *ted3 det1-1*, *ted3 DET1*, and *TED3*ox proteins are in lanes 1 to 5, respectively.

fairly weak phenotype; i.e., it is slow-growing and smaller in size than wild-type plants (*14*). F_1 progeny exhibited conditional synthetic growth defects (in strong light, Fig. 3H), and double mutants showed embryonic lethality, further substantiating the close functional relations between DET1 and peroxisomes.

Supporting the view that *ted3* may encode a hypermorphic mutation contributing to the restoration of peroxisomal activities, some phenotypic similarities were observed between *ted3* and plants overexpressing *TED3* (*TED3*ox) (*16*). In each case, light-grown seedlings had hypocotyls longer than the wild-type and were less responsive, albeit to different degrees, to the inhibition of hypocotyl elongation by light (Fig. 3I). To better understand the nature of the *ted3* mutation, we compared the level of some glyoxysomal enzymes, namely, isocitrate lyase (ICL), malate synthase (MS), and peroxisomal ascorbate peroxidase (pAPX), in wild-type, *det1-1*, and *ted3* plants. In dark-grown seedlings, the amount of these enzymes in *ted3 det1* is markedly higher than in *det1-1* (Fig. 3J, left). Although the RNAs were expressed at similar levels in light-grown wild-type and *ted3* seedlings (*12*), their protein levels were much higher in *ted3* and *TED3*ox than in wild-type (Fig. 3J, right). These results suggest that the *ted3* mutation may be hypermorphic and that it contributes to the stabilization of some peroxisomal proteins.

The profound suppression of *det1* by *ted3* prompted us to compare global gene expression profiles in wild-type, *det1-1* and *ted3* plants with the use of the *Arabidopsis* oligoarray that contains ~8300 genes (*17*). In dark-grown seedlings, over 900 genes were misregulated by more than threefold in *det1-1* compared with wild-type, whereas the expression of ~90% of them was restored or partially restored by *ted3* (Fig. 4A). In the light, of the over 300 genes with expression altered threefold or greater in *det1-1*, ~60% were restored to various degrees in *ted3 det1-1* (Fig. 4B). A significant portion of the genes suppressed by *ted3* is associated with various stress responses, including light stress (Fig. 4C, table S1), which suggests that *det1* mimics a light-stressed seedling. In addition, a number of peroxisomal genes and genes with functions related to peroxisomes were underexpressed in *det1-1*, including genes encoding alanine:glyoxylate aminotransferase, isocitrate lyase, glyoxylate II, and oleosin. Genes highly overexpressed included those encoding peroxisomal-3-ketoacyl-CoA thiolase, malate dehydrogenase, and the putative peroxisome proliferation factor PEX11 (table S1).

We have provided evidence that increased peroxisomal function can suppress the numerous morphological and gene-expression defects caused by mutations in *DET1*. Although the precise mechanism of its function is unknown, DET1 is a nuclear protein associated with chromatin, and it probably acts to regulate the expression of hundreds of genes by limiting promoter access to transcription factors (*18*). TED3/AtPex2p might act directly in a photomorphogenetic pathway negatively regulated by DET1, which includes the regulation of genes required for peroxisomal functions. This loss of regulation of peroxisomal gene expression in *det1* mutants would result in defective peroxisomes, which may cause seedlings to de-etiolate. In the hypermorphic *ted3* mutant, increased peroxisomal functions may lead to restoration of etiolation. Given the putative functions of PEX2, the mutant ted3 protein may increase trafficking and stabilization of peroxisomal proteins. Most misregulated genes are restored to their normal expression levels by *ted3*, which suggests that there are signals generated from peroxisomes that regulate nuclear gene expression through negative feedback, because peroxisomes are known to release signal molecules to affect nuclear gene expression (*19*). The fact that *ted3* partially suppressed another pleiotropic de-etiolated mutant, *cop1* (Fig. 4D), but not *det2*, a de-etiolated mutant defective in brassinosteroid biosynthesis (*5*), indicates that this model may apply more generally to a photomorphogenetic pathway controlled by the DET1, COP, and FUS proteins. COP proteins control photomorphogenesis by mediating proteolysis of key transcriptional regulators, thereby limiting transcription factor availability to light-regulated promoters (*2*). Given the similar phenotypes of *det1*, *cop*, and *fus* mutants, and the fact that *cop1* mutants also show some peroxisomal defects in sugar and IBA response assays (*12*), DET1 and the COP proteins may act to regulate similar sets of genes with roles in light signaling, photosynthesis, and peroxisomal function.

Given the hypermorphic nature of the *ted3* mutation, it is also possible that *ted3* suppresses *det1* indirectly. Because *det1* mutants exhibit many characteristics of light-stressed plants (*3*) (table S1), it is conceivable that increasing peroxisomal function might allow *det1 ted3* plants to manage light stress more effectively (*20*). This possibility seems less likely, because it is known that a number of stress conditions induce the proliferation of peroxisomes (*21*) rather than reduce their function as in the *det1* mutant. Thus, the suppression of *det1* by *ted3* appears specific, not general, to the mutant phenotypes. Identification of *ted3* as a mutant with increased peroxisomal function will be invaluable in elucidating the functions of PEX proteins in peroxisomal biogenesis and for addressing the roles of peroxisomes in the light signaling and stress response pathways of plants.

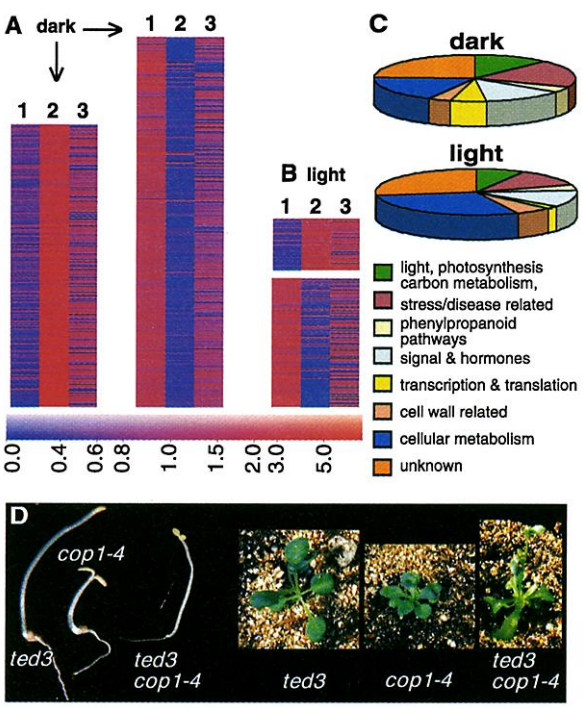

Fig. 4. *ted3* rescues the abnormal expression of many genes in *det1-1* and partially suppresses *cop1*. (**A** and **B**) Cluster analysis of genes induced or repressed at least threefold in *det1-1* in the dark (A) or light (B). Color bar (bottom) indicates relative expression level. 1, wild-type; 2, *det1-1*; 3, *ted3 det1-1*. (**C**) Classification of genes whose aberrant expression in *det1-1* was restored or partially restored by *ted3*. (**D**) *cop1* is partially suppressed by *ted3*. Shown are 6-day dark-grown (left) and 20-day light-grown (right) plants.

References and Notes

1. M. M. Neff, C. Fankhauser, J. Chory, *Genes Dev.* **14**, 257 (2000).
2. C. Schwechheimer, X. W. Deng, *Semin. Cell Dev. Biol.* **11**, 495 (2000).
3. J. Chory, C. Peto, R. Feinbaum, L. Pratt, F. Ausubel, *Cell* **58**, 991 (1989).
4. A. Pepper, T. Delaney, T. Washburn, D. Poole, J. Chory, *Cell* **78**, 109 (1994).
5. A. E. Pepper, J. Chory, *Genetics* **145**, 1125 (1997).
6. A ~4.5-kb Sac I–Sal I fragment containing *ted3* was cloned into pzp211, a vector described by P. Hajdukiewicz, Z. Svab, and P. Maliga [*Plant Mol. Biol.* **25**, 989 (1994)].
7. S. Subramani, *Physiol. Rev.* **78**, 171 (1998).

T. L. Johnson, L. J. Olsen, *Plant Physiol.* **127**, 731 (2001).
9. A ~700-bp Sal I–Pst I GFP fragment and a ~1.1-kb Kpn I–Sal I *TED3* cDNA fragment (EST F6H9T7, ABRC, Ohio State University) were cloned into pCHF3 containing the 35S promoter (C. Fankhauser, J. Chory, unpublished data).
10. A Sac I–Sal I *TED3* cDNA fragment was cloned into pCHF3.
11. A ~700-bp Sal I–Bam HI fragment containing the promoter and the first 43 nucleotides of the coding sequence of *TED3* was cloned into the *GUS* gene fusion plasmid pBI101.3 (Clontech, Palo Alto, CA).
12. J. Hu, J. Chory, unpublished data.
M. Hayashi, K. Toriyama, M. Kondo, M. Nishimura, *Plant Cell* **10**, 183 (1998).
B. K. Zolman, I. D. Silva, B. Bartel, *Plant Physiol.* **127**, 1266 (2001).
15. Cotyledons grown for 5 days in light were fixed for 21 hours at 4°C with 2.5% glutaraldehyde, 2% paraformaldehyde, and 3.75% acrolein in phosphate buffer and were processed as described H-m. Li, K. Culligan, R.A. Dixon, and J. Chory [*Plant Cell* **7**, 1599 (1995)].
16. A ~1.1-kb Kpn I–Sal I *TED3* cDNA fragment was cloned into pCHF3.
17. Chip experiment was conducted using 5-day dark- or light-grown seedlings according to the instructions from Affymetrix (Santa Clara, CA). Cluster analysis was performed using GeneSpring 4.1.1 (Silicon Genetics, Redwood City, CA).
18. D. Schroeder *et al.*, *Curr. Biol.*, in press.
19. F. J. Corpas, J. B. Barroso, L. A. del Rio, *Trends Plant Sci.* **6**, 145 (2001).
20. P. Mullineaux, L. Ball, C. Escobar, B. Karpinska, G. Creissen, S. Karpinski, *Philos. Trans. R. Soc. London Ser. B* **355**, 1531 (2000).
E. Lopez-Huertas, W. Charlton, B. Johnson, I. Graham, A. Baker, *EMBO J.* **19**, 6770 (2000).
A. Konieczny, F. M. Ausubel, *Plant J.* **4**, 403 (1993).
23. K. Boudonck, L. Dolan, P. J. Shaw, *J. Cell Sci.* **111**, 3687 (1998).
24. We thank M. Chen, D. Schroeder, and Y. Zhao for comments on the manuscript; D. Trelease for the catalase and pAPX antiserum; J. Harada for the ICL and MS antiserum; and B. Bartel and X. W. Deng for the *pxa1* and *cop1* seeds. Supported by a National Science Foundation grant to J.C. and the Howard Hughes Medical Institute.

Supporting Online Material
www.sciencemag.org/cgi/content/full/297/5580/405/DC1
Table S1

6 May 2002; accepted 17 June 2002

Integrin-Mediated Long-Term B Cell Retention in the Splenic Marginal Zone

Theresa T. Lu and Jason G. Cyster*

The mechanisms that control localization of marginal zone (MZ) B cells are poorly understood. Here we show that MZ B cells express elevated levels of the integrins LFA-1 (αLβ2) and α4β1 and that they bind to the ligands ICAM-1 and VCAM-1. These ligands are expressed within the MZ in a lymphotoxin-dependent manner. Combined inhibition of LFA-1 and α4β1 causes a rapid and selective release of B cells from the MZ. Furthermore, lipopolysaccharide-triggered MZ B cell relocalization involves down-regulation of integrin-mediated adhesion. These studies identify key requirements for MZ B cell localization and establish a role for integrins in peripheral lymphoid tissue compartmentalization.

Most blood that enters the spleen is released into the marginal sinus; from there, it flows through the macrophage- and B cell–rich MZ, before it returns to the circulation through venous sinuses (*1*, *2*). This enormous flow of blood ensures that B cells situated in the MZ, which includes the bulk of splenic B cells in humans (*3*), readily come in contact with systemic antigens. B cell entry into the MZ compartment is regulated by B cell receptor signaling (*4*, *5*), and the compartment is enriched for immunoglobulin M–positive (IgM^+) memory B cells (*6*) and cells that react with bacterial antigens (*7*) and autoantigens (*8*–*10*). The sessile, nonrecirculatory state of MZ B cells (*3*) contrasts with the migratory state of follicular B cells and suggests that the mechanisms that control their localization are likely to be distinct. Consistent with this, the chemokine/receptor pair CXCL13 (BLC)/CXCR5, which is critical for B cell migration to lymphoid follicles (*11*) and to the body cavities (*12*), is not needed for B cell lodgment within the MZ. Therefore, we considered whether B cells may lodge in the MZ in response to other factors and investigated the contribution of adhesion molecules. Measurement of surface integrin levels on MZ B cells, which account for about 5% of spleen B cells in C57BL/6 mice, revealed elevated expression of αL and β2 integrin subunits on MZ B cells compared with follicular B cells. Thus, MZ B cells have higher amounts of the αLβ2 heterodimer LFA-1 (Fig. 1A). MZ B cells also expressed greater amounts of β1-containing integrins than follicular B cells, but they had equal levels of α4-containing and lower levels of β7-containing integrins (Fig. 1A). Staining with an antibody specific for α4β7 revealed lower expression of this heterodimer on MZ B cells (Fig. 1A). Although antibodies specific for murine α4β1 are not available, the only known partners for α4 are β1 and β7. Therefore, we conclude that MZ B cells express higher levels of α4β1 than follicular B cells.

We next tested the functional status of LFA-1 and α4β1 on MZ and follicular B cells with an ex vivo adhesion assay (*13*). MZ B cells bound substantially better than follicular B cells to the LFA-1 ligand ICAM-1 and to the α4β1 ligand VCAM-1 (Fig. 1B). Adhesion to ICAM-1 could be inhibited by a blocking antibody to αL, which confirms the role of LFA-1 and rules out contributions by other β2 integrins (Fig. 1B). Similarly, adhesion to VCAM-1 could be inhibited with an antibody to α4 (Fig. 1B). Although α4β7 can also function as a receptor for VCAM-1, an α4β7-neutralizing antibody did not block adhesion of MZ B cells to VCAM-1 (*14*). The MZ is located adjacent to the CXCL13-rich follicle and, after being released in the MZ, recirculating follicular B cells migrate to the follicle in response to CXCL13 (*11*). Therefore, we examined how the relative differences between follicular and MZ B cell integrin activity influenced CXCL13-mediated chemotaxis. MZ and follicular B cells showed similar dose sensitivities for CXCL13 (Fig. 1C), although the maximal MZ B cell response was typically lower than the response of follicular cells. When we compared the chemotactic response of cells on uncoated and on VCAM-1–coated Transwell filters, MZ B cell migration was strongly retarded in the presence of VCAM-1, whereas follicular B cell migration was enhanced (Fig. 1C). Previous studies in other systems have shown that optimal integrin-ligand densities enhance cell motility, but, at densities above a critical threshold, migration is retarded (*15*). Our findings indicate that, at ligand densities that augment follicular B cell migration, the high levels of functional integrins on MZ B cells are sufficient to prevent cells from migrating to CXCL13.

We next examined the functional relevance of LFA-1 and α4β1 to MZ B cell localization in vivo. Three hours after we treated mice with a combination of α4 and αL blocking antibodies, MZ B cell numbers in the spleen were reduced and large numbers of MZ phenotype B cells were present in the blood (Fig. 2, A and B). This effect was specific for MZ B cells, because follicular B cell numbers in the spleen showed no change

Howard Hughes Medical Institute, Department of Microbiology and Immunology, and Division of Pediatric Immunology and Rheumatology, University of California, 513 Parnassus Avenue, San Francisco, CA 94143, USA.

*To whom correspondence should be addressed. E-mail: cyster@itsa.ucsf.edu